

Microlensing Constraints on the Stellar and Planetary Mass Functions

JENNIFER C. YEE¹ AND SCOTT J. KENYON¹

¹*Center for Astrophysics | Harvard & Smithsonian, 60 Garden St., Cambridge, MA 02138, USA*

ABSTRACT

The mass function (MF) of isolated objects measured by microlensing consists of both a stellar and a planetary component. We compare the microlensing MFs of Gould et al. (2022) and Sumi et al. (2023) to other measurements of the MF. The abundance of brown dwarfs in the Sumi et al. (2023) stellar MF is consistent with measurements from the local solar neighborhood (Kirkpatrick et al. 2024). Microlensing free-floating planets (μ FFPs) may be free-floating or orbit host stars with semimajor axes $a \gtrsim 10$ au and therefore can constrain the populations of both free-floating planetary-mass objects and wide-orbit planets. Comparisons to radial velocity and direct imaging planet populations suggest that either most of the μ FFP population with masses $> 1 M_{\text{Jup}}$ is bound to hosts more massive than M dwarfs or some fraction of the observed bound population actually comes from the low-mass tail of the stellar population. The μ FFP population also places strong constraints on planets inferred from debris disks and gaps in protoplanetary disks observed by ALMA.

1. INTRODUCTION

Measurements of the microlensing free-floating planet (μ FFP) population (Mróz et al. 2020a; Ryu et al. 2021; Gould et al. 2022; Koshimoto et al. 2023; Sumi et al. 2023) have broad implications for both the stellar and planetary mass functions (MFs) and theories of their formation. Current theories for the formation of planets and stars differ in significant ways. Stars grow at the center of a collapsing molecular cloud; planets grow within a disk of material orbiting a newly-formed star (e.g. Shu et al. 1987; Drazkowska et al. 2023; Pineda et al. 2023). These systems evolve as planets migrate, interact, or get ejected from their parent systems either during or after the planet formation process. We consider the connections between the μ FFP population, the wide-orbit planet population, and the stellar initial MF (IMF), which have implications for constraining the evolution of the planetary systems and theories of their formation.

The properties of the μ FFP population are inferred by measuring deviations from extrapolating the stellar MF to planetary masses. Because the two populations are measured together, we can decompose objects into separate populations of stars and planets and then investigate the mass range where the stellar and planetary mass functions converge. Unlike most microlensing planets, μ FFPs do not have a microlensing signal from a host star. They could be true free-floating objects or planets on very wide orbits with semimajor axes $\gtrsim 10$ au. Despite this ambiguity, the population of bone-fide free-floating planetary-mass objects (PMOs) and the set of wide-orbit planets must be subsets of the μ FFP population. These features of μ FFPs provide limits on the low-mass end of the stellar population and the high-mass end of the planet population.

There is considerable confidence in assigning most objects to either the stellar or planetary population based on their masses. However, there is much more ambiguity for objects with masses $\sim 3\text{--}15 M_{\text{Jup}}$, where M_{Jup} is the mass of Jupiter (e.g., Burrows et al. 1997; Schlaufman 2018; Kirkpatrick et al. 2024, and references therein). Improving our understanding of the frequency of objects in this mass range may yield better constraints on the lowest (highest) masses generated by star (planet) formation processes.

For stars, the microlensing stellar MF can be compared with the mass function of the lowest mass brown dwarfs derived from surveys of the nearest stellar objects (e.g., Kirkpatrick et al. 2024). For planets, the μ FFP population can be compared to the wide-orbit planet populations derived from radial velocity and direct imaging observations. μ FFPs also test constraints on the population of Jupiter-mass planets inferred from studies of debris disks and protoplanetary disks.

Clanton & Gaudi (2017) also tried to reconcile wide-orbit planets with the μ FFP population. Sumi et al. (2011) had inferred a large population of free-floating Jupiters based on an excess of short-timescale ($t_E < 1$ day) microlensing events. Clanton & Gaudi (2017) tested whether the observations could be explained by the bound planet population derived in Clanton & Gaudi (2016) from microlensing (Gould et al. 2010; Sumi et al. 2010), radial velocity (Montet et al. 2014), and direct imaging (Lafrenière et al. 2007; Bowler et al. 2015) measurements of the planet frequency. The constraints available at that time from radial velocity and direct imaging were relatively weak and limited to planets somewhat more massive than Jupiter.

Since then, the measurements of the μ FFP populations have been updated several times. Mróz et al. (2017) found no evidence for a large population of free-floating Jupiters in their timescale distribution, although they did find tentative evidence of a population of free-floating super-Earths. Gould et al. (2022) made an independent measurement based on the Einstein radius distribution and constrained both the frequency and power-law index of the μ FFP population. Sumi et al. (2023) combined timescale and Einstein radius distributions to measure those properties for a larger sample of events. In addition, several techniques (radial velocities, microlensing, direct imaging, and coherent structures in circumstellar disks) have provided new insights into the frequency and mass distribution of planetary mass objects at 10–100 au distances from a host star (e.g., Poleski et al. 2021; Pearce et al. 2022; Bae et al. 2023; Currie et al. 2023; Lagrange et al. 2023).

We compare the MFs inferred from μ FFPs (Gould et al. 2022; Sumi et al. 2023) to the wide-orbit planet populations inferred from other techniques. We begin with a description of our methodology and then discuss the constraints on μ FFPs and brown dwarfs from the microlensing perspective. After comparing these constraints to constraints from direct imaging and radial velocity surveys for massive planets, we discuss indirect constraints from structures observed in debris and protoplanetary disks. We conclude with a brief summary.

Table 1. Mass/Spectral-Type Ranges Based on Pecaut & Mamajek (2013)

Sp Type	Pecaut & Mamajek (2013)			Vigan et al. (2021)	
	Mass Range (M_{\odot})	Pop. Frac		Mass Range (M_{\odot})	Pop. Frac
		Chabrier (2005)	Sumi et al. (2023)		Chabrier (2005)
B	[2.43, 8.00]	0.025	0.034	[1.68, 3.00]	0.032
A	[1.68, 2.43]	0.022	0.027		
F	[1.07, 1.68]	0.056	0.058		
G	[0.89, 1.07]	0.035	0.035	[0.58, 1.68]	0.198
K	[0.58, 0.89]	0.107	0.099		
M	[0.08, 0.58]	0.743	0.537	[0.30, 0.58]	0.229

NOTE—Population fractions normalized to the number (0.08, 8) M_{\odot} stars in the Chabrier (2005) MF. B stars are limited to $M_* < 8 M_{\odot}$. Vigan et al. (2021) divided their stars into BA, FGK, and M groups as indicated by the horizontal lines. The values provided are the combined values for each group limited to $0.3 M_{\odot} < M_* < 3 M_{\odot}$ stars.

2. METHODOLOGY

2.1. Stars vs. Planets

Because the μ FFP population is fit as an excess to the stellar population, we can separate the microlensing MFs into stellar and planetary components. We refer to brown dwarfs as the low-mass tail of the stellar formation process and planets as any objects from the planetary component of the MF, regardless of mass.

For our quantitative comparisons, we quote the planet frequencies as number of planets per 100 stars (following the conventions of Fulton et al. 2021). We define stars to be objects in the range $0.08 M_{\odot} < M_* < 8 M_{\odot}$. That is, we assume that neither brown dwarfs ($M < 0.08 M_{\odot}$) nor high-mass stars ($M_* > 8 M_{\odot}$) form a significant number of planets. We use the Chabrier (2005) MF as our reference stellar MF. We restrict our comparisons to objects with semi-major axis $a > 10$ au and focus on objects with masses m_p (or $m_p \sin i$) $< 13 M_{\text{Jup}}$. We use M_* for the masses of host stars, m_p for masses of the companions, and M for masses of objects in a mass function.

For studies that quote planet frequencies for a particular spectral type or types rather than a host mass range, we use Pecaut & Mamajek (2013) to derive assumed mass ranges for a given spectral type. Table 1, lists the fraction of stars in each spectral type bin from the Chabrier (2005) MF. For studies that cover host stars from only part of the range, we consider either the scenario that those hosts are representative of all stars or re-weight the frequencies by the fraction of $0.08 M_{\odot} < M_* < 8 M_{\odot}$ stars represented by those hosts.

2.2. Radial Velocity & Direct Imaging

For radial velocity and direct imaging, the distinction between planets and brown dwarfs is unclear, especially for objects with masses $m_p \sim 3 - 15 M_{\text{Jup}}$. For radial velocity studies, it may be possible to separate planets and brown dwarf companions based on mass ratio. Because direct imaging studies are still limited to detecting the most massive companions, the origin of many companions is ambiguous unless the companion lies within a disk (Bowler et al. 2025; Close et al. 2025; Zhou et al. 2025) or with additional coplanar objects (e.g., the HR 8799 system Marois et al. 2008, 2010) or both (e.g., β Pic b and c Lagrange et al. 2009, 2019).

We will compare the population of objects with masses $< 13 M_{\text{Jup}}$ detected by radial velocity and direct imaging to the μ FFP population. If there are more radial velocity and direct imaging companions than μ FFPs, we can infer the fraction of such companions that should be classified as planetary vs. as brown dwarfs. Having fewer radial velocity and direct imaging companions than μ FFPs places a constraint on the fraction of μ FFPs that are bound vs. free-floating.

2.3. Circumstellar Disks

To generate the structures observed in protoplanetary and debris disks, embedded or nearby planets are one option among many (Vorobyov et al. 2020; Friebe et al. 2022; Smallwood et al. 2023; Stuber et al. 2023). Massive planets

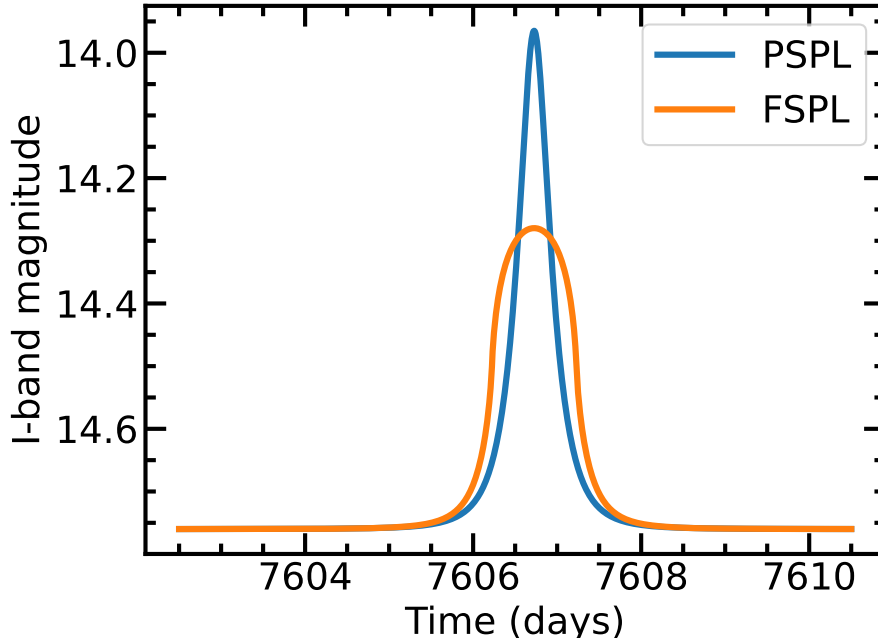


Figure 1. An example of the microlensing light curve of a μ FFP based on the properties of OGLE-2016-BLG-1540 (Mróz et al. 2018). The Einstein timescale of the event is $t_E = 0.320$ day. The blue curve shows the light curve under a point-source approximation (PSPL). The orange curve includes the effect of the physical extent of the source star (FSPL), which enables a measurement of the Einstein radius.

outside a disk can create spiral density waves (Dong et al. 2011; Cimerman & Rafikov 2021). Inside the disk, planets can clear out material along their orbits and also generate spiral waves throughout the disk. The contrast of these features relative to the rest of the disk constrains the mass of the planet and its distance from the disk and the host star.

In most cases, the presumed planets are at large distances from the host star; their frequency can then be directly compared with the frequency of microlensing FFPs. Most studies assume that every circumstellar disk structure (e.g., each gap in an ALMA disk) corresponds to a single planet. If there are more inferred companions than allowed by the μ FFP population, this assumption is invalidated, which constrains the physics used to infer the planet properties. If there are fewer inferred companions, a significant fraction of the μ FFP population can then be unbound rather than in wide-orbits.

3. MICROLENSING CONSTRAINTS ON THE FREE-FLOATING PLANET POPULATION

3.1. Overview of Microlensing FFP Detection & Characterization

A microlensing event occurs when a foreground object, the lens, passes in front of and magnifies the light from a (usually unrelated) background object, the source. The morphology of the resulting light curve depends on the Einstein radius, θ_E , and Einstein timescale, t_E , which are proportional to the square root of the lens mass, M (Paczynski 1986):

$$\theta_E = \sqrt{\kappa M \pi_{\text{rel}}} = 2.0 \mu\text{as} \left(\frac{M}{10 M_{\oplus}} \right)^{1/2} \left(\frac{\pi_{\text{rel}}}{0.016 \text{ mas}} \right)^{1/2} \quad (1)$$

$$t_E = \frac{\theta_E}{\mu_{\text{rel}}} = 0.12 \text{ d} \left(\frac{M}{10 M_{\oplus}} \right)^{1/2} \left(\frac{\mu_{\text{rel}}}{6 \text{ mas/yr}} \right)^{-1} \quad (2)$$

where $\kappa = 8.14 M_{\odot}^{-1} \text{ mas}$, $\pi_{\text{rel}} \equiv \text{au}(D_L^{-1} - D_S^{-1})$, D_L is the distance to the lens, D_S is the distance to the source, and μ_{rel} is the lens-source relative proper motion. Microlensing experiments monitor the brightness of millions of stars to look for this particular light curve morphology (Gaudi 2012).

Equations 1 and 2 indicate that a planetary mass object will produce a microlensing event with a short timescale and will have a small θ_E (if it is measurable). Figure 1 shows example light curves based on the μ FFP event OGLE-2016-BLG-1540 (Mróz et al. 2018). Because the event was caused by a single body, it is a point-lens (PL) event, which had $t_E = 0.32$ day, $\theta_E = 9.2 \mu\text{as}$, and a Neptune-mass lens. The blue curve (PSPL) shows the light curve assuming a point source (PS). The orange curve (FSPL) includes the finite source (FS) effect (i.e., accounting for the physical extent of the source star), which is one way to measure θ_E (Yoo et al. 2004).

A microlensing event that appears as a single lens event due to a planetary-mass object may lack a microlensing signature due to the host star. Given a detected planet, the probability of detecting a host star decreases rapidly with the orbital separation of the planet. For a planet that appeared to be separated from its host star by $6.6 \theta_E$ (analogous to a Neptune-like orbit), there is only a $\sim 20\%$ probability of detecting the microlensing signature of the host star (Gould 2016; Clanton & Gaudi 2017). For individual μ FFP candidates, the microlensing light curve is usually only sufficient to rule out host stars within ~ 10 au (Mróz et al. 2018, 2020a; Ryu et al. 2021), making it ambiguous whether any given μ FFP candidate is truly free-floating or merely on a wide orbit.

High-resolution follow-up observations can be used to search for potential host stars, but such searches are still in the early stages. For example, Mróz et al. (2024) searched for hosts for five μ FFP candidates, but were only able to rule out the most massive $\sim 10\text{--}35\%$ of possible host stars.

Even without knowing whether or not there are host stars for individual objects, the μ FFP population measures the combined sum of the wide-orbit planet population and the population of free-floating PMOs. For example, if all μ FFPs are wide orbit planets, there cannot be any true FFPs and vice versa. Based on published limits on host stars for individual events, we set 10 au as the lower bound of the semi-major axis range probed by μ FFPs.

Equations 1 and 2 also show that while short t_E or small θ_E events are strong candidates for having planetary mass lenses, the mass of any given object is ambiguous. Hence, the properties of the μ FFP population are inferred by measuring statistically significant excesses to the t_E or θ_E distributions after accounting for the stellar population. The first μ FFP population studies measured or constrained excesses to the t_E distribution (Sumi et al. 2011; Mróz et al. 2017). The studies discussed in this work have measured the θ_E distribution, which has fewer unknowns but is restricted to a smaller sample of events. Relatively few objects with small θ_E have been detected (Mróz et al. 2018, 2019, 2020b,a; Kim et al. 2021; Ryu et al. 2021; Koshimoto et al. 2023; Jung et al. 2024).

3.2. Measurements of the Microlensing FFP Population

Recently, both the Korea Microlensing Telescope Network (KMTNet; Kim et al. 2016) and Microlensing Observations in Astrophysics (MOA; Bond et al. 2004) surveys have made measurements of the μ FFP MF using samples that include events with measured θ_E .

Gould et al. (2022) measured a power-law distribution for μ FFPs from a statistical sample of 30 events with measured θ_E , including 4 detections in the “planetary” regime ($\lesssim 10 \mu\text{as}$ in their case). In particular, they observed an absence of objects with $9 \mu\text{as} < \theta_E < 26 \mu\text{as}$, which they dubbed the “Einstein Gap.” Because of this gap, they suggested that the MF could be comprised of two separate MF, one for “planets” and one for “stars”. For the planetary component, they derive

$$\frac{dN}{d \log M} = \frac{0.28 \pm 0.09}{\text{dex} \times \text{stars}} \times \left(\frac{M}{38 M_{\oplus}} \right)^{-p} \quad (3)$$

with p likely to be in the range $0.9 < p < 1.2$; $p = 0.6$ is ruled out.

Gould et al. (2022) showed that the μ FFP population is consistent with the short timescale events from Mróz et al. (2017) and with the bound microlensing planet population from Poleski et al. (2021), who measured the occurrence rate of planets from 5 – 15 au to be $1.4^{+0.9}_{-0.6}$ per star with a power law index of $p \sim 1.0$. Gould et al. (2022) also found consistency between their population and limits on the population of ‘Oumuamua-like objects and the fraction of Uranus and Neptune-like objects that would be detected as free-floating vs. bound planets.

Sumi et al. (2023) conducted a joint statistical analysis of events from the MOA survey (Koshimoto et al. 2023), some with measured θ_E and others with only t_E . They derived a similar power-law mass function to Gould et al. (2022):

$$\frac{dN}{d \log M} = \frac{2.18^{+0.52}_{-1.40}}{\text{dex} \times \text{stars}} \times \left(\frac{M}{8 M_{\oplus}} \right)^{-p} \quad ; \quad p = 0.96^{+0.47}_{-0.27}. \quad (4)$$

Figure 2 compares the MF from Gould et al. (2022) and Sumi et al. (2023). Both studies quote their MFs in planets per star. Sumi et al. (2023) defines stars as objects from their stellar MF with $3 \times 10^{-4} M_{\odot} < M < 8 M_{\odot}$. We

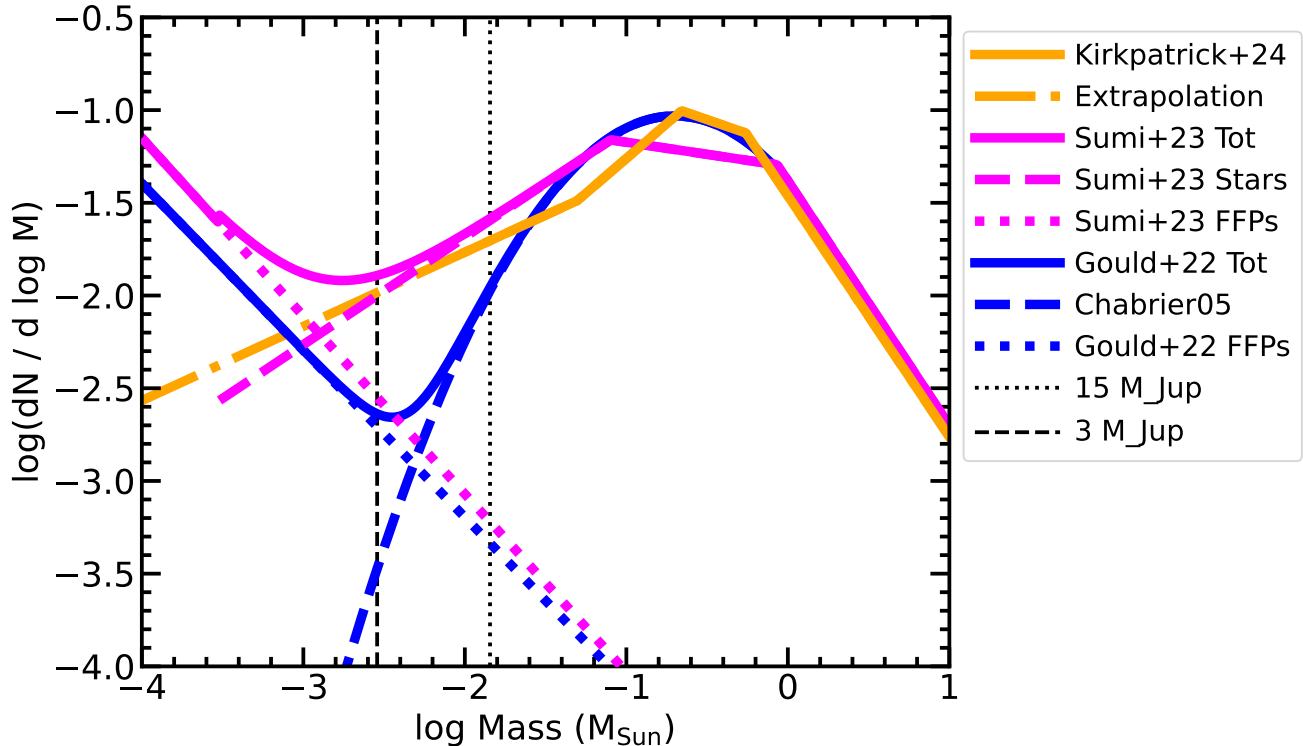


Figure 2. Mass functions from Gould et al. (2022) and Chabrier (2005), Sumi et al. (2023) (magenta), and Kirkpatrick et al. (2024) (orange). The dashed lines show the FFP component while the dotted lines show the stellar component. The solid line shows their sum. The orange dash-dot line indicates the Kirkpatrick et al. (2024) MF is extrapolated beyond the available data below $10^{-2} M_{\odot}$. The black, vertical, dashed and dotted lines are drawn at $3 M_{\text{Jup}}$ and $15 M_{\text{Jup}}$, respectively. Although this regime is often considered to be “planetary” (as defined by mass), in these mass functions, the “stellar” component is clearly dominant.

renormalize the Sumi et al. (2023) MF to have equal numbers of stars in this range as in the Chabrier (2005) MF. Gould et al. (2022) does not specify a particular mass range as corresponding to stars, so we use the same range as for Sumi et al. (2023) to renormalize the MF. Because stellar MFs are steep at both low and high masses, the normalization is relatively insensitive to the choices of the upper and lower limits. Using $0.013 M_{\odot}$ as the lower limit or $100 M_{\odot}$ as the upper limit changes the normalization by $< 1\%$.

3.3. Comparison of Sumi et al (2023) Stellar MF With Other MFs

The stellar MF of Sumi et al. (2023) consists of a 3-part power law and differs from Chabrier (2005) below $\sim 1 M_{\odot}$. Figure 2 shows that Sumi et al. (2023) predicts fewer M dwarfs and significantly more brown dwarfs than Chabrier (2005), but the MFs agree well for higher-mass stars. These features are quantified in spectral-type bins in Table 1. For comparison, we also plot the IMF from Kirkpatrick et al. (2024) in Figure 2. This comparison shows that the abundance of brown dwarfs identified in the Sumi et al. (2023) MF is consistent with observations of the MF in the Solar neighborhood. All three stellar MFs are reasonably consistent with each other except in the brown dwarf regime.

We choose to quote all of our planet frequencies, including those for the Sumi et al. (2023) μ FFP MF, relative to the number of $0.08 M_{\odot} < M < 8 M_{\odot}$ stars from the Chabrier (2005) MF. If we were to use the Sumi et al. (2023) stellar MF instead, there would be $\sim 20\%$ fewer $0.08 M_{\odot} < M < 8 M_{\odot}$ stars or $\sim 25\%$ more planets per star.

Table 2. Number of Objects per 100 Stars

Mass Range	Gould et al. (2022)			Sumi et al. (2023)		
	Total	FFPs	Stars	Total	FFPs	Stars
Convenient Divisions:						
[1 M_{Jup} , 13 M_{Jup}]	4.2	2.4	1.9	17.4	3.4	13.9
[1 M_{Sat} , 1 M_{Jup}]	5.1	5.1	0.0	10.2	8.2	2.0
[1 M_{Nep} , 1 M_{Sat}]	28.4	28.4	0.0	50.1	50.1	0.0
[1 M_{Earth} , 1 M_{Nep}]	430.9	430.9	0.0	888.1	888.1	0.0
“Giant” Planets:						
[1 M_{Sat} , 13 M_{Jup}]	9.3	7.5	1.9	27.6	11.7	15.9
[1 M_{Nep} , 13 M_{Jup}]	37.8	35.9	1.9	77.7	61.8	15.9
[1 M_{Nep} , 1 M_{Jup}]	33.6	33.6	0.0	60.3	58.3	2.0
Comparisons to Other Work:						
[13 M_{Jup} , 80 M_{Jup}]	27.8	0.2	27.6	33.7	0.1	33.6
[5 M_{Jup} , 13 M_{Jup}]	2.0	0.4	1.6	8.1	0.5	7.7
[1 M_{Jup} , 75 M_{Jup}]	30.0	2.6	27.4	49.2	3.6	45.6
[1 M_{Jup} , 20 M_{Jup}]	6.6	2.4	4.2	22.6	3.6	19.0

NOTE—Normalized to the number $(0.08, 8) M_{\odot}$ stars in the Chabrier (2005) MF.

3.4. Comparison of Gould et al (2022) & Sumi et al (2023) Microlensing FFP MFs

Figure 2 shows the Sumi et al. (2023) μ FFP MFs, and Table 2 presents integrated frequencies over various mass ranges. We list the total number of objects in each mass range, as well as separating them into the planetary and stellar components. For simplicity, we do not include uncertainties in the MFs in our calculations: for Gould et al. (2022), we assume $p = 0.9$ and for Sumi et al. (2023), we calculate frequencies for $p = 0.96$.

While the two MFs have a similar slope, the estimates of the μ FFP frequencies from Gould et al. (2022) are a factor of ~ 1.5 to 2 smaller than the values derived from Sumi et al. (2023). However, given the Poisson uncertainties in the Gould et al. (2022) measurement (4 observed FFPs), these values are roughly consistent. Even with these uncertainties, Table 2 indicates there are multiple small planets ($< 1 M_{\text{Nep}}$) per star in wide orbits or ejected from their parent systems, whereas there is < 1 wide-orbit planet or free-floating PMO with a mass in the range $(1 M_{\text{Nep}}, 13 M_{\text{Jup}})$ per star.

4. COMPARISON TO OTHER MEASUREMENTS OF THE WIDE-ORBIT PLANET POPULATION

4.1. Direct Imaging

Attempts to detect exoplanets with direct imaging benefit from increasingly sophisticated and sensitive AO cameras and high quality software (cf. Currie et al. 2023). However, direct imaging has only been sensitive to the very highest mass end of the “planetary” mass regime: $m_p > 1$ to a few M_{Jup} . In microlensing populations, the planet and brown dwarf populations overlap at these masses (Fig. 2). We can test whether the direct imaging planet population is consistent with being planetary by seeing whether it can be explained by the μ FFP population or whether it also requires contributions of objects from the stellar population.

4.1.1. Nielsen et al (2019)

Nielsen et al. (2019) analyze GPI data for 300 stars, which yielded 6 planets and 3 brown dwarfs. The host stars range in mass from $0.2 M_{\odot}$ to $5 M_{\odot}$. Nielsen et al. (2019) fit their population with a power law:

$$d^2 N / (dm_p da) \propto m_p^{\alpha} a^{\beta}. \quad (5)$$

For the full host sample, they derive $\alpha = -2.3^{+0.8}_{-0.7}$. This power-law index ($\alpha \equiv -(p+1)$) is consistent with the values for the microlensing FFP population.

Nielsen et al. (2019) infer raw frequencies of 2.1–5.4 (68% confidence interval) 5–13 M_{Jup} companions per 100 stars with $0.2 M_{\odot} < M_* < 5 M_{\odot}$. For comparison, Gould et al. (2022) calculate the total frequency of 5–13 M_{Jup} objects as 2.0 per 100 stars from a combination of FFPs and brown dwarfs. From Sumi et al. (2023), we infer a total frequency of 8.1 objects per 100 stars with the majority coming from the tail of the stellar population (see Table 2). If we assume the results for $0.2 M_{\odot}$ to $5 M_{\odot}$ stars are representative of all stars, the Nielsen et al. (2019) frequencies are only consistent with the microlensing population if most of the companions are drawn from the brown dwarf population.

However, stars from $0.2 M_{\odot}$ to $5 M_{\odot}$ account for only $\sim 65\%$ of the stellar population. If we assume that no stars outside of this mass range have 5–13 M_{Jup} companions, the frequency is reduced to $2.3_{-0.9}^{+1.2}$ planets per 100 stars. This result is still in tension with the hypothesis that all of these companions are planets.

One way to reconcile these frequencies would be to use the lower limit from Nielsen et al. (2019) from the 95% confidence interval: 1.1 planets per 100 stars. Combined with the correction factor for the fraction of hosts and the uncertainties in the μ FFP population, this may be enough to bring the measurements into agreement. But, it also requires that *all* of the μ FFPs in this mass range are bound, wide-orbit planets.

All of the planets in Nielsen et al. (2019) orbit stars with $M_* > 1.5 M_{\odot}$ ($\sim 40\%$ of their sample), so they also analyze this subsample of stars. They find a similar power-law index to the full sample and a frequency of 5–13 M_J companions at 10–100 au to be 9_{-4}^{+5} planets per 100 stars with $1.5 M_{\odot} < M_* < 5 M_{\odot}$. Such a large frequency of planets, if it extended to host stars of all masses, is inconsistent with the μ FFP population. However, 1.5–5 M_{\odot} stars account for only about $\sim 6\%$ of the stellar population. Assuming no other stars have companions of this mass, which is supported by the lack of detections around lower-mass stars, the planet frequency from Nielsen et al. (2019) becomes $0.5_{-0.2}^{+0.3}$ planets per 100 stars. This frequency is in good agreement with the μ FFP population but still requires all μ FFPs to be bound planets.

Nielsen et al. (2019) also measure the frequency of companions in the 13–80 M_{Jup} range (the commonly used mass range for brown dwarfs). After scaling according to the host-star population (0.2 – $5.0 M_{\odot}$), the frequency of such objects is $0.5_{-0.3}^{+0.5}$ objects per 100 stars. These values are roughly consistent with the Gould et al. (2022) and Sumi et al. (2023) μ FFP populations (0.2 and 0.1 planets per 100 stars, respectively). It also suggests that the vast majority of microlensing objects in this mass range cannot be bound to a star, which is consistent with the hypothesis that they are part of the tail of the stellar MF.

4.1.2. Vigan et al (2021)

Vigan et al. (2021) analyze SPHERE results for 105 stars and are sensitive to 1–75 M_{Jup} companions over the semi-major axis range $a = 5$ – 300 au. They conclude that the predicted fraction of the population due to planets vs. brown dwarfs is a function of stellar mass: a large fraction of substellar companions are drawn from the planetary MF for BA stars, while for M stars, most companions are drawn from the stellar MF. Vigan et al. (2021) report their results as the frequency of systems, which represents a lower limit on the frequency of planets, if stars can host multiple planets (as in the case of HR8799).

Vigan et al. (2021) derive the frequencies of at least one substellar ($1 M_{\text{Jup}} < m_p < 75 M_{\text{Jup}}$) companion as $23.0_{-9.7}^{+13.5}$ (BA stars), $5.8_{-2.8}^{+4.7}$ (FGK stars), and $12.6_{-7.1}^{+12.9}$ (M stars) per 100 stars.

To obtain the total companion frequency, we re-weight each spectral-type bin based on the fraction of the stellar population it corresponds to (Table 1). The mass ranges for the M and BA bins are truncated because Vigan et al. (2021) state their sample is limited to host stars with $0.3 M_{\odot} < M_* < 3 M_{\odot}$.

After correcting for these population fractions and assuming no stars outside the range $0.3 M_{\odot} < M_* < 3 M_{\odot}$ have companions, the Vigan et al. (2021) results imply a total frequency of $2.0_{-1.4}^{+2.7}$ substellar companions per 100 stars. These values are comparable to the expected FFP population from microlensing: 2.6 planets per 100 stars (Gould et al. 2022) and 3.6 planets per 100 stars (Sumi et al. 2023). See Table 2. However, as with Nielsen et al. (2019), if we assume that all of these companions correspond to the μ FFPs, then all of the μ FFPs must be bound. If we consider the Vigan et al. (2021) sample to be representative of all stars (instead of excluding planets around stars with $M_* < 0.3 M_{\odot}$ or $M_* > 3 M_{\odot}$), the frequencies increase by a factor of 2.

Similar to microlensing studies, Vigan et al. (2021) consider their direct imaging detections as a mix of planets and brown dwarfs. We scale the parameterized population models from Vigan et al. (2021) by the host star population fraction and assume that no stars with $M_* < 0.3 M_{\odot}$ or $M_* > 3 M_{\odot}$ have companions. The total frequencies are $\geq 0.5_{-0.3}^{+3.4}$ planets per 100 stars and $\geq 2.0_{-1.4}^{+2.7}$ brown dwarfs per 100 stars. Even with the factor of 2 correction, these frequencies are below the limits inferred from μ FFPs and the microlensing stellar MF, respectively. Because the

microlensing stellar population is much larger than the [Vigan et al. \(2021\)](#) brown dwarf sample, this result implies that a significant fraction of the microlensing objects either do not have host stars or orbit stars with masses outside the range $0.3 M_{\odot} < M_* < 3 M_{\odot}$ (see Table 2).

The one caveat is that [Vigan et al. \(2021\)](#) assumed fixed power-law MFs with $\beta = -1.31$ (where $\beta \equiv -(p + 1)$) for the planetary MF, which is shallower than allowed for the microlensing FFP population ([Gould et al. 2022](#)). A steeper power-law would decrease the number of larger mass objects in the planetary component of the [Vigan et al. \(2021\)](#) population, but the number of observed objects and total frequencies remain fixed. This alternative implies a larger frequency of brown dwarfs and smaller frequency of planets than considered above; however, the results remain consistent with the microlensing populations.

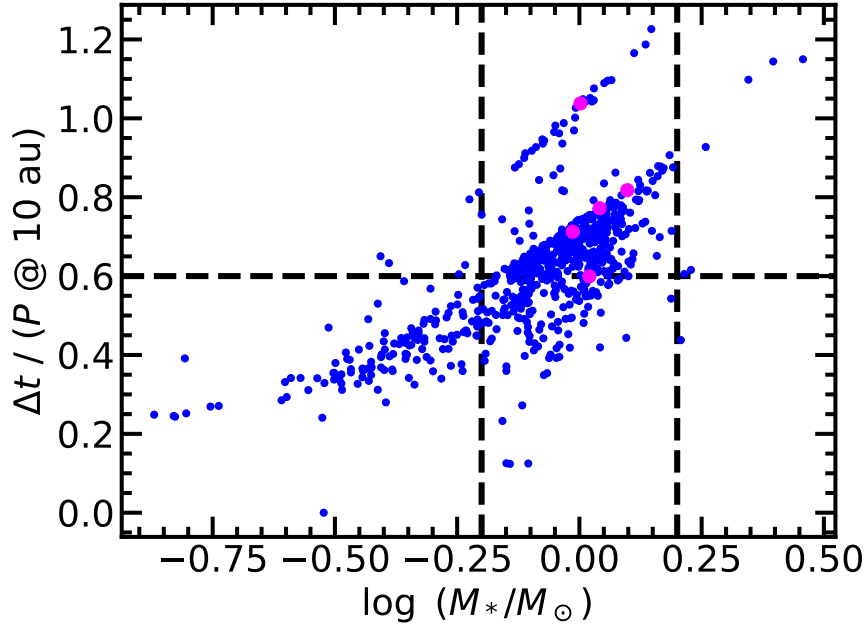


Figure 3. Comparison of host mass ($\log M$) and the duration of observations Δt as a fraction of the period P at $a = 10$ au for the radial velocity sample from Rosenthal et al. (2021) and Fulton et al. (2021). Blue points are for all stars. Magenta points indicate stars with planets with $a > 10$ au. The horizontal dashed line at $y = 0.6$ is roughly the minimum for detected $a > 10$ au planets. The vertical dashed lines are drawn at $\log M = -0.2, 0.2$.

4.2. Radial Velocity: Fulton et al (2021)

Radial velocity planet searches offer another technique to probe the wide-orbit planet population via direct detections. Several recent radial velocity measurements of the giant planet population “beyond the ice line” (Fernandes et al. 2019; Wittenmyer et al. 2020; Fulton et al. 2021) indicate that the frequency of gas giants appears to increase with a out to 3–10 au and then drop. Of these, only Fulton et al. (2021) claims sensitivity to planets beyond 10 au, so we focus our comparison on those results.

Fulton et al. (2021) analyze a sample of 719 stars containing 178 planets from the California Legacy Survey (Rosenthal et al. 2021). Based on their figure 9, we estimate the frequency of $1 - 20 M_{\text{Jup}}$ objects in orbits from 10–50 au as $6.3^{+3.0}_{-1.9}$ planets per 100 stars (median and 68% confidence interval), and the frequency of $5 M_{\text{Jup}} - 13 M_{\text{Jup}}$ objects in orbits from 10–100 au is $3.5^{+2.3}_{-1.6}$ planets per 100 stars. The values for the μFFP population from Table 2 for these mass ranges lie at the extreme edge of the probability distributions in figure 9 from Fulton et al. (2021), indicating the measurements are inconsistent.

Fulton et al. (2021) describe the sample as consisting of FGKM stars, corresponding to most stars; renormalizing the values to account for stars with $M_* > 1.68 M_{\odot}$ has minimal effect on the totals. However, the sample has low completeness beyond 10 au. Because of Kepler’s third law, the completeness could be correlated with host mass. To test this possibility, we use the data from Rosenthal et al. (2021) to calculate the total duration of observations, Δt , for each star. We divide this by the period, P , at 10 au for that star to determine the fraction of the orbital period that has been observed. Figure 3 shows that there is indeed a strong correlation between this fraction and the host mass.

Figure 3 also highlights the five companions in the sample with $a > 10$ au and $m \leq 13 M_{\text{Jup}}$. The minimum value of $\Delta t / (P @ 10 \text{ au})$ is ~ 0.6 . If we assume the sample is only complete for stars above this value, then the range of host masses probed by Fulton et al. (2021) for wide-orbit planets is approximately $-0.2 < \log M_*/M_{\odot} < 0.2$ or $0.63 M_{\odot} < M_* < 1.58 M_{\odot}$. Stars in this range account for only 17% of all stars.

Applying this correction factor to the Fulton et al. (2021) frequencies, yields $1.1^{+0.5}_{-0.3}$ objects with masses $1 M_{\text{Jup}} < m < 20 M_{\text{Jup}}$ in orbits from 10–50 au per 100 stars and $0.6^{+0.4}_{-0.3}$ objects with masses $5 M_{\text{Jup}} < m_p < 13 M_{\text{Jup}}$ in orbits from 10–100 au per 100 stars. These values are consistent with the μFFP population. But for the $5 M_{\text{Jup}} <$

$m_p < 13 M_{\text{Jup}}$ bin, if all such objects are planets, all μFFPs in this mass range must be bound. Also, no technique should detect planets of this mass around stars with masses outside the range $0.63 M_{\odot} < M_* < 1.58 M_{\odot}$ because they should not exist. If they do exist, a significant fraction of the [Fulton et al. \(2021\)](#) objects are brown dwarfs rather than planets.

5. COMPARISON TO PLANETS INFERRED FROM DISK STRUCTURES

5.1. Debris Disks: [Pearce et al \(2022\)](#)

Although many direct imaging surveys do not yield a planet, they often detect scattered light from a debris disk (e.g., [Esposito et al. 2020](#)). These detections provide one way to indirectly infer the presence of planets and their properties. [Stuber et al. \(2023\)](#) demonstrate that a planet orbiting inside a debris disk sculpts the inner disk in a way that allows observations to infer the mass of the planet. [Friebe et al. \(2022\)](#) also illustrate gap structures imposed on a debris disk by migrating planets of different masses. Planets may also induce other kinds of disk structures such as warps or spiral density waves.

[Pearce et al. \(2022\)](#) use the morphologies of debris disks around 178 host stars to constrain the masses of the planets assumed to be sculpting them. They consider the minimum planet required to stir the disk and maintain its inner edge at a fixed distance from the host star. Constraints for maintaining the inner edge of the disk are stronger; we use these estimates for our comparison of planet populations.

Figure 4 shows the cumulative distribution of the population of planets from [Pearce et al. \(2022\)](#) assuming the inner edge of the disk is sculpted by a single planet. We restrict the planet population to those planets with semi-major axes $a > 10$ au (158 planets with a maximum semi-major axis of 300 au). Planet masses range from $0.012 M_{\text{Jup}}$ to $7 M_{\text{Jup}}$ with a median planet mass of $0.4 M_{\text{Jup}}$.

We also show the cumulative distributions in spectral type bins (M/K/G/F/Massive) according to the ranges given in Table 1 and the minimum and maximum host masses in the sample. The host stars in [Pearce et al. \(2022\)](#) have masses ranging from $0.22 M_{\odot}$ to $3.7 M_{\odot}$ but are heavily biased toward stars with masses exceeding $0.8 M_{\odot}$; the sample contains only four M dwarfs. The inferred planet minimum mass distribution is a strong function of host mass. However, after shifting all the distributions by the median planet mass (bottom panels), a Kolmogorov-Smirnov test shows no significant differences between them.

The top panel of Figure 4 compares various power-laws to the [Pearce et al. \(2022\)](#) cumulative distribution. The power-laws are normalized to match the [Pearce et al. \(2022\)](#) distribution at $\log(m_p/M_{\text{Jup}}) = -0.7$ and 0.0 ($0.2 M_{\text{Jup}}$ and $1 M_{\text{Jup}}$). A power-law index of $p = 1.0$, as suggested by the μFFP population, is clearly too steep for the inferred debris disk population. This difference could be resolved if there is a large population of small objects found as μFFPs that are not associated with a debris disk structure.

Table 3 lists planet frequencies for the [Pearce et al. \(2022\)](#) population. We count the number of planets (N_{pl}) in a given planet mass (m_p) and spectral type (SpT) bin and calculate the fraction of planets (frac) of this type. We weight this frequency by the fraction of the stellar population ‘‘Pop Frac.’’ represented by the range of host masses in that bin ($\min M_*$, $\max M_*$) to derive the predicted number of planets per 100 stars (‘‘All’’). This estimate would be the total planet frequency if we assume the sample of stars with debris disks is representative of the planet population around all stars. We also consider an additional weight to account for the debris disk frequency, assuming DD Frac. = 10%, 25%, and 50% for M, FGK, and AB stars, respectively ([Lestrade et al. 2009](#)). The resulting values are given in the ‘‘DD-only’’ column and are the minimum frequencies assuming that stars without debris disks have no planets. We sum the values to obtain the total predicted number of planets in various mass bins, which are given in Table 4.

For the mass ranges $1 M_{\text{Jup}} < m_p < 13 M_{\text{Jup}}$ and $1 M_{\text{Sat}} < m_p < 1 M_{\text{Jup}}$, the frequency is 3.5 and 8.1 planets per 100 stars, respectively, for the [Pearce et al. \(2022\)](#) sample. These values are similar to the values from the μFFP populations (see Table 2). However, they require that all of the μFFPs in this range are bound planets, although this requirement can be relaxed if only stars with debris disks have planets of this type.

The [Pearce et al. \(2022\)](#) masses are lower limits on the masses of the planets. Because the estimates of the [Pearce et al. \(2022\)](#) planet frequency for $m_p > M_{\text{Sat}}$ are already roughly equivalent to the μFFP population, it is difficult for them to be significantly more massive than the minimum values. As an extreme example, we predict 16.2 total planets with $1 M_{\text{Earth}} < m_p < 13 M_{\text{Jup}}$ per 100 stars from [Pearce et al. \(2022\)](#). If all of them actually had masses between $1 M_{\text{Jup}}$ and $13 M_{\text{Jup}}$, that would vastly exceed the allowable totals from the μFFP population. We estimate that $\lesssim 25\%$ of the [Pearce et al. \(2022\)](#) planets with minimum masses $< 1 M_{\text{Jup}}$ can have true masses $> 1 M_{\text{Jup}}$, even

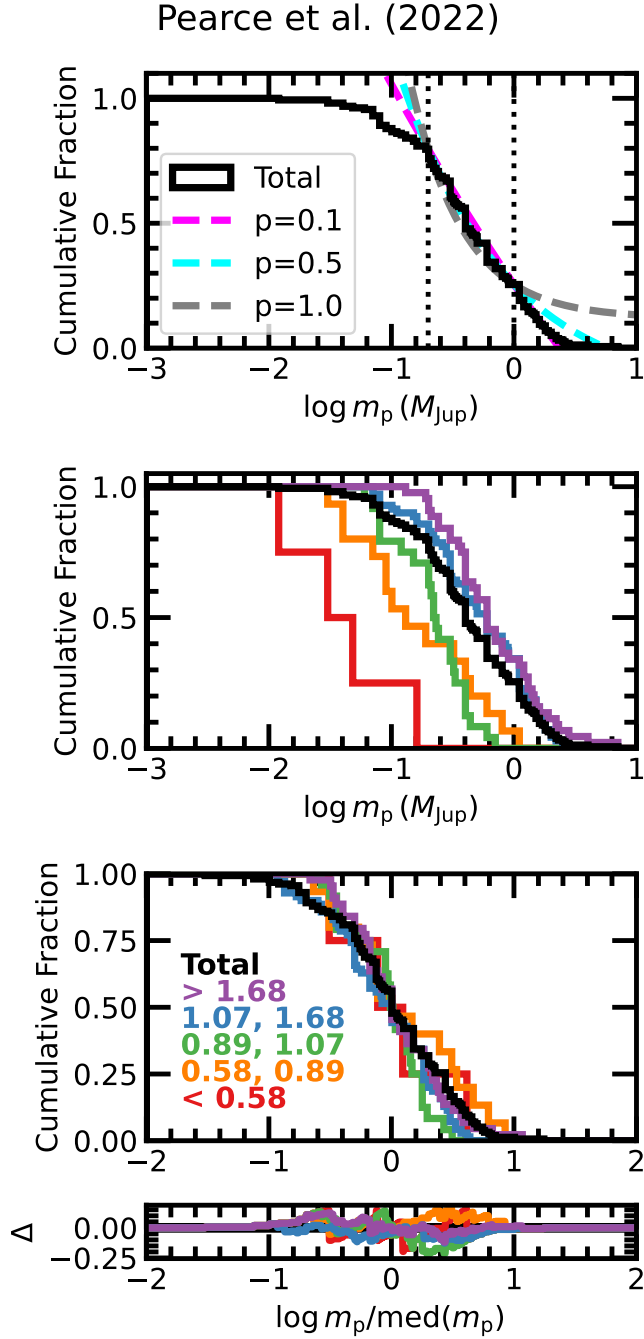


Figure 4. Cumulative distributions of minimum planet masses from Pearce et al. (2022) assuming the inner disk edge is sculpted by a single planet. The distribution for the full sample is shown in black, while the subsamples for different spectral types are shown in color (red=M, blue=K, green=G, blue=F, purple=A/B). The top and middle panels show the normalized cumulative distributions. Power-laws with various indices ($dN/d\log M_p \propto M_p^{-p}$) are shown in the top panel, normalized to fit the observed distribution at the points indicated by the dotted lines. The bottom panels show the inferred debris-disk planet distributions shifted by the median mass for each group and the difference of the shifted distributions relative to the full sample.

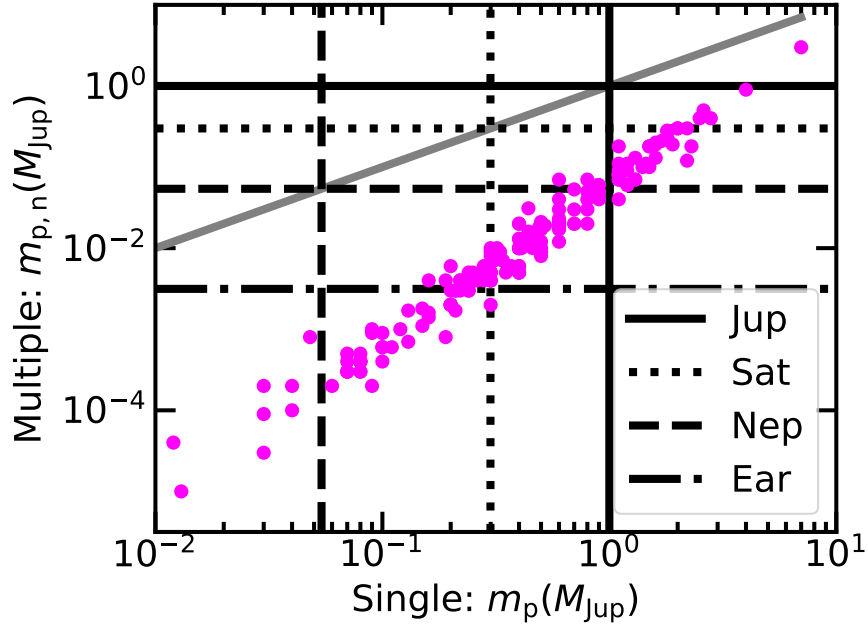


Figure 5. Magenta points compare the minimum masses calculated by Pearce et al. (2022) for a single planet to shape the disk (m_p , x-axis) vs. multiple, equal-mass planets ($m_{p,n}$, y-axis). Gray solid line is 1-to-1. Black lines show masses of solar system planets (see legend).

including the assumption that all planets in the $1 M_{\text{Jup}} < m_p < 13 M_{\text{Jup}}$ bin have true masses $> 13 M_{\text{Jup}}$. Thus, the μ FFP population can place upper limits on the masses of the planets predicted from debris disk physics.

The alternative is that the inner edges of the disks are sculpted by multiple planets. Pearce et al. (2022) conclude that the minimum masses for multiple, equal mass planets to maintain the inner edge of the disk are generally at least an order of magnitude smaller than for a single planet (see Figure 5), and the majority of the planets have masses $m_p < 1M_{\text{Sat}}$. Pearce et al. (2022) do not calculate the total number of planets required for each disk, so we cannot directly compare the frequencies or the resulting cumulative distributions with the microlensing results. Depending on how many planets are required, this scenario may be more compatible with the microlensing results.

5.2. ALMA Substructure

As summarized in Najita et al. (2022), recent ALMA observations divide protostellar disks around solar-type stars into two general classes (see also ALMA Partnership et al. 2015; Avenhaus et al. 2018; Huang et al. 2018; Long et al. 2019; Cieza et al. 2019; van der Marel & Mulders 2021; Bae et al. 2023, and references therein). The youngest solar-type stars all have a compact disk with a radius of 20–30 au. Roughly 25% of these young stars have thin rings of gas and dust at larger radii. Rings have typical widths, $\delta a/a \approx 0.05\text{--}0.10$, and lie at distances $a \approx 40\text{--}200$ au from the host star (Hughes et al. 2018; Bae et al. 2023; Michel et al. 2023; Huang et al. 2024, and references therein). For robust ALMA detections, the rings are massive, $\gtrsim 5\text{--}10 M_{\oplus}$ of solids in the form of mm-sized to cm-sized pebbles. There are also rings in transitional disk systems, where the compact disk has an inner hole (e.g., Bae et al. 2023, and references therein). A small sample of protostellar disks have spirals or crescents (van der Marel et al. 2021; Bae et al. 2023).

The gaps seen in ALMA disks probe the planet population at a much younger age (see also Andrews et al. 2016; Sheehan et al. 2020; Teague et al. 2021). In this section, we consider four works that calculate properties for planets required to open the observed gaps in protoplanetary disks: Zhang et al. (2018) (Section 5.2.1), Lodato et al. (2019) (Section 5.2.2), Wang et al. (2021) (Section 5.2.3), and Zhang et al. (2023) (Section 5.2.4). We discuss our conclusions in Section 5.2.5.

For the four studies discussed below, we calculate the expected number of planets per 100 stars for each study. Each sample spans a range of stellar masses. However, the total number of stars in each sample is small, and there

Table 3. Planets per 100 Stars of a given Spectral Type from [Pearce et al. \(2022\)](#)

SpT	min M_*	max M_*	N_{stars}	Pop Frac.	DD Frac.
M	0.22	0.58	4	0.355	0.25
Planet Mass Range	N_{pl}	frac	All	DD-only	
[1 M_{Jup} , 13 M_{Jup}]	0	0.000	0.0	0.0	
[1 M_{Sat} , 1 M_{Jup}]	0	0.000	0.0	0.0	
[1 M_{Nep} , 1 M_{Sat}]	1	0.250	8.9	2.2	
[1 M_{Earth} , 1 M_{Nep}]	3	0.750	26.6	6.7	
Total:	4	1.000	35.5	8.9	
SpT	min M_*	max M_*	N_{stars}	Pop Frac.	DD Frac.
K	0.58	0.89	17	0.107	0.25
Planet Mass Range	N_{pl}	frac	All	DD-only	
[1 M_{Jup} , 13 M_{Jup}]	1	0.059	0.6	0.2	
[1 M_{Sat} , 1 M_{Jup}]	5	0.294	3.1	0.8	
[1 M_{Nep} , 1 M_{Sat}]	6	0.353	3.8	0.9	
[1 M_{Earth} , 1 M_{Nep}]	3	0.176	1.9	0.5	
Total:	15	0.882	9.4	2.4	
SpT	min M_*	max M_*	N_{stars}	Pop Frac.	DD Frac.
G	0.89	1.07	26	0.035	0.25
Planet Mass Range	N_{pl}	frac	All	DD-only	
[1 M_{Jup} , 13 M_{Jup}]	0	0.000	0.0	0.0	
[1 M_{Sat} , 1 M_{Jup}]	10	0.385	1.3	0.3	
[1 M_{Nep} , 1 M_{Sat}]	14	0.538	1.9	0.5	
[1 M_{Earth} , 1 M_{Nep}]	0	0.000	0.0	0.0	
Total:	24	0.923	3.2	0.8	
SpT	min M_*	max M_*	N_{stars}	Pop Frac.	DD Frac.
F	1.07	1.68	82	0.056	0.50
Planet Mass Range	N_{pl}	frac	All	DD-only	
[1 M_{Jup} , 13 M_{Jup}]	24	0.293	1.6	0.8	
[1 M_{Sat} , 1 M_{Jup}]	28	0.341	1.9	1.0	
[1 M_{Nep} , 1 M_{Sat}]	18	0.220	1.2	0.6	
[1 M_{Earth} , 1 M_{Nep}]	0	0.000	0.0	0.0	
Total:	70	0.854	4.8	2.4	
SpT	min M_*	max M_*	N_{stars}	Pop Frac.	DD Frac.
Massive	1.68	3.70	49	0.039	0.50
Planet Mass Range	N_{pl}	frac	All	DD-only	
[1 M_{Jup} , 13 M_{Jup}]	15	0.306	1.2	0.6	
[1 M_{Sat} , 1 M_{Jup}]	22	0.449	1.8	0.9	
[1 M_{Nep} , 1 M_{Sat}]	7	0.143	0.6	0.3	
[1 M_{Earth} , 1 M_{Nep}]	0	0.000	0.0	0.0	
Total:	44	0.898	3.5	1.8	

NOTE—The header of each section gives the properties of the host stars. N_{pl} is the number of $a > 10$ au in a particular mass range and, “frac” is N_{pl} divided by the total number of such planets at all semi-major axes. Because some of the inferred objects have $m_{\text{p}} > 13 M_{\text{Jup}}$, the “frac” total may be < 1 . “All” is the number of objects per 100 stars assuming the [Pearce et al. \(2022\)](#) sample represents the planet population for all stars. “DD-only” assumes that the sample represents only those with debris disks, i.e., other stars do not have planets.

does not appear to be a strong correlation between inferred planet mass and host mass. Hence, we do not re-weight the sample by spectral type/stellar mass bin, but instead assume the frequency is independent of stellar mass. In addition, for consistency with previous calculations, we limit the proposed planets to those in gaps at $R_{\text{gap}} \geq 10$ au. The calculations of the planet frequencies are given in [Table 5](#) and the cumulative distributions of the inferred planet populations are shown in [Figure 6](#).

Table 4. Total Planets per 100 Stars from Pearce et al. (2022)

Planet Mass Range	N_{pl}	frac	All	DD-only
$[1 M_{\text{Jup}}, 13 M_{\text{Jup}}]$	40	0.225	3.5	1.6
$[1 M_{\text{Sat}}, 1 M_{\text{Jup}}]$	65	0.365	8.1	3.0
$[1 M_{\text{Nep}}, 1 M_{\text{Sat}}]$	46	0.258	16.3	4.5
$[1 M_{\text{Earth}}, 1 M_{\text{Nep}}]$	6	0.034	28.5	7.1
$[5 M_{\text{Jup}}, 13 M_{\text{Jup}}]$	1	0.006	0.1	0.0

NOTE— N_{pl} is the number of $a > 10$ au in a particular mass range and, ‘frac’ is N_{pl} divided by the total number of such planets at all semi-major axes. ‘All’ is the number of objects per 100 stars assuming the Pearce et al. (2022) sample represents the planet population for all stars. ‘DD-only’ assumes that the sample represents only those with debris disks, i.e., other stars do not have planets.

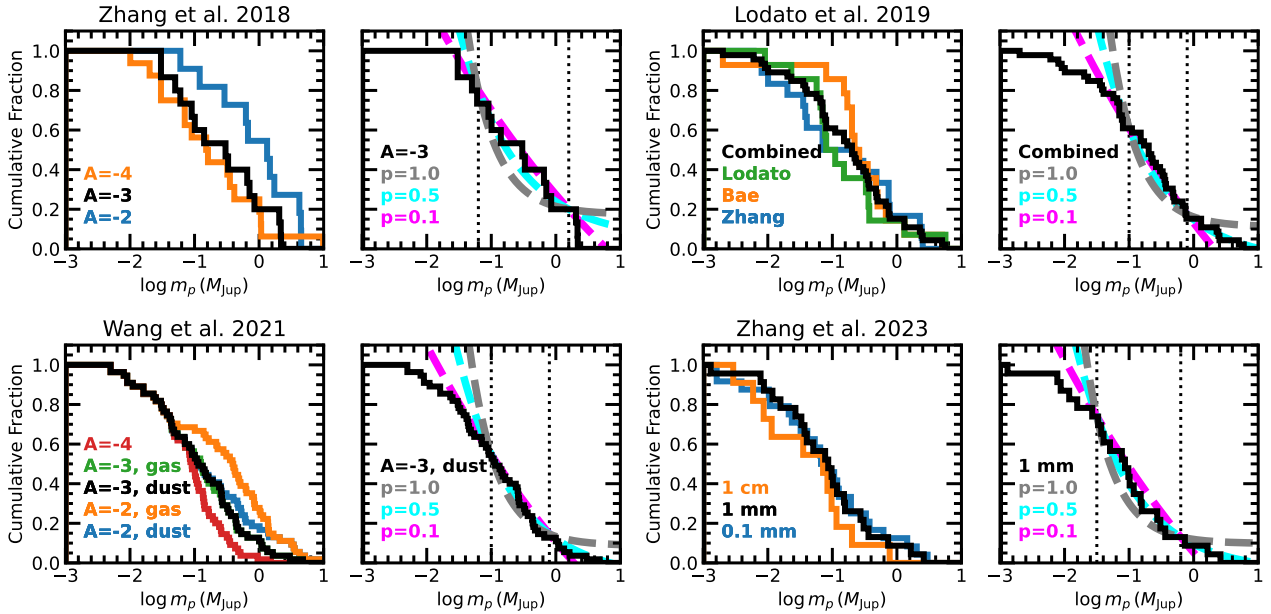


Figure 6. Cumulative distribution functions of planets inferred from ALMA disks from Zhang et al. (2018) (upper left), Lodato et al. (2019) (upper right), Wang et al. (2021) (lower left), and Zhang et al. (2023) (lower right). The left panel in each pair shows distributions for different assumptions of physics from each study (for Zhang et al. 2018 and Wang et al. 2021: $A \equiv \log \alpha$, Zhang et al. 2023: different limits for the maximum grain size) or, in the case of Lodato et al. (2019), different observational samples (see legend). The right panel shows one of those distributions relative to power-laws with different indices p , normalized to the points indicated by the vertical dotted lines.

5.2.1. Zhang et al (2018)

Zhang et al. (2018) took a sample of 14 protoplanetary disks from the DSHARP survey (Andrews et al. 2018) containing a total of 19 gaps. Using hydrodynamical simulations under different assumptions for the disk turbulent viscosity coefficient, α , they map the properties of the gaps to planet masses (for the legend in Figure 6, we use $A \equiv \log \alpha$). In this sample, there are 40–50 planets per 100 stars with $a \geq 10$ au between $1 M_{\text{Sat}}$ and $13 M_{\text{Jup}}$

Table 5. Planets per 100 Stars Inferred from ALMA Disks

Zhang et al. (2018)										
	$\alpha = 10^{-2}$		$\alpha = 10^{-3}$		$\alpha = 10^{-4}$					
Total Planets:	11		15		15					
Total Stars:	14		14		14					
Mass Range	N_{pl}	freq	N_{pl}	freq	N_{pl}	freq				
[1 M_{Jup} , 13 M_{Jup}]	5	35.7	2	14.3	3	21.4				
[1 M_{Sat} , 1 M_{Jup}]	2	14.3	5	35.7	3	21.4				
[1 M_{Nep} , 1 M_{Sat}]	3	21.4	4	28.6	5	35.7				
[1 M_{Earth} , 1 M_{Nep}]	0	0.0	3	21.4	4	28.6				
[5 M_{Jup} , 13 M_{Jup}]	0	0.0	0	0.0	1	7.1				
Lodato et al. (2019)										
	T1: Taurus		T2: Zhang et al. (2018)		T3: Bae et al. (2018)		Combined			
Total Planets:	15		18		13		46			
Total Stars:	10		14		9		33			
Mass Range	N_{pl}	freq	N_{pl}	freq	N_{pl}	freq	N_{pl}	freq		
[1 M_{Jup} , 13 M_{Jup}]	2	20.0	2	14.3	2	22.2	6	18.2		
[1 M_{Sat} , 1 M_{Jup}]	3	30.0	5	35.7	4	44.4	12	36.4		
[1 M_{Nep} , 1 M_{Sat}]	7	70.0	3	21.4	6	66.7	16	48.5		
[1 M_{Earth} , 1 M_{Nep}]	2	20.0	7	50.0	0	0.0	9	27.3		
[5 M_{Jup} , 13 M_{Jup}]	1	10.0	0	0.0	0	0.0	1	3.0		
Wang et al. (2021) ^a										
	$\alpha = 10^{-2}$, dust		$\alpha = 10^{-2}$, gas		$\alpha = 10^{-3}$, dust		$\alpha = 10^{-3}$, gas		$\alpha = 10^{-4}$	
Total Planets:	54		54		54		54		54	
Total Stars:	35		35		35		35		35	
Mass Range	N_{pl}	freq	N_{pl}	freq	N_{pl}	freq	N_{pl}	freq	N_{pl}	freq
[1 M_{Jup} , 13 M_{Jup}]	9	25.7	14	40.0	6	17.1	6	17.1	1	2.9
[1 M_{Sat} , 1 M_{Jup}]	9	25.7	15	42.9	9	25.7	9	25.7	7	20.0
[1 M_{Nep} , 1 M_{Sat}]	16	45.7	8	22.9	20	57.1	20	57.1	26	74.3
[1 M_{Earth} , 1 M_{Nep}]	19	54.3	16	45.7	19	54.3	19	54.3	20	57.1
[5 M_{Jup} , 13 M_{Jup}]	2	5.7	2	5.7	0	0.0	0	0.0	0	0.0
Zhang et al. (2023)										
	$\alpha_{\text{max}} = 0.1$ mm		$\alpha_{\text{max}} = 1$ mm		$\alpha_{\text{max}} = 1$ cm					
Total Planets:	24		22		10					
Total Stars:	15		15		15					
Mass Range	N_{pl}	freq	N_{pl}	freq	N_{pl}	freq				
[1 M_{Jup} , 13 M_{Jup}]	2	13.3	2	13.3	0	0.0				
[1 M_{Sat} , 1 M_{Jup}]	3	20.0	2	13.3	1	6.7				
[1 M_{Nep} , 1 M_{Sat}]	8	53.3	8	53.3	4	26.7				
[1 M_{Earth} , 1 M_{Nep}]	8	53.3	9	60.0	4	26.7				
[5 M_{Jup} , 13 M_{Jup}]	0	0.0	0	0.0	0	0.0				

^aIn this table, the choice of “dust” vs. “gas” refers only to ambiguous gaps, which may be in either category. See text.

NOTE—Because some of the inferred companions have $m_{\text{p}} > 13 M_{\text{Jup}}$, “Total Planets” may exceed the sum of the N_{pl} column.

regardless of the assumed value of α . This frequency is well in excess of the number allowed by the μFFP population in this mass range: 7.5 (Gould et al. 2022) and 11.7 (Sumi et al. 2023) planets per 100 stars.

5.2.2. Lodato et al (2019)

Instead of using detailed hydrodynamical simulations, [Lodato et al. \(2019\)](#) use a simple assumption that the gap width scales with the Hill radius of a planet. They calculate the masses of the hypothetical planets existing in several, non-overlapping, samples of observed proto-planetary disks: their own sample of disks from Taurus, the DSHARP sample from [Zhang et al. \(2018\)](#), and a compilation of gaps from [Bae et al. \(2018\)](#). Table 5, lists the number of planets per star for each of their samples and also for the combination. As with the [Zhang et al. \(2018\)](#) sample, the number of planets per star between $1 M_{\text{Sat}}$ and $13 M_{\text{Jup}}$ is well in excess of the number allowed by the μFFP populations.

5.2.3. Wang et al (2021)

[Wang et al. \(2021\)](#) take the calculations of [Lodato et al. \(2019\)](#) one step further and consider whether the observed gap in the dust disk is likely to have a corresponding gap in the gas disk. Planets below a certain mass only open gaps in the dust disk; the Hill radius relation of [Lodato et al. \(2019\)](#) should apply (the “dust” regime). However, planets above this mass are likely to open gaps in the gas disk and are therefore governed by the empirical relation of [Kanagawa et al. \(2016\)](#) (the “gas” regime). That relation generally implies more massive planets than the Hill radius relation for the same gap width.

For each dust gap in their sample, [Wang et al. \(2021\)](#) classify it according to which regime applies or whether it is ambiguous. For our calculations of the number of planets per star, we perform two sets of calculations for each value of α . First, we assume that the ambiguous gaps are all in the “dust” regime, and then we assume that they are all in the “gas” regime. Thus, the labels in Figure 6 and Table 5 refer to the distinction only for the gaps in the ambiguous regime, rather than completely separating the populations by the assumed underlying physics. For the $A \equiv \log \alpha = -4$ regime, there are no ambiguous gaps, so we give only one set of values.

Regardless of the choice for ambiguous planets, there is significant tension with the μFFP population. The microlensing results allow for 2.4 ([Gould et al. 2022](#)) and 3.4 ([Sumi et al. \(2023\)](#)) large gas giants ($1 M_{\text{Jup}} < m_p < 13 M_{\text{Jup}}$) and 5.1 and 8.2 medium gas giants ($1 M_{\text{Sat}} < m_p < M_{\text{Jup}}$) per 100 stars, respectively. Even with Poisson statistics and regardless of the assumed physics, the inferred gap populations from [Wang et al. \(2021\)](#) imply too many large planets relative to the μFFP population.

5.2.4. Zhang et al (2023)

[Zhang et al. \(2023\)](#) calculate the inferred mass of planets for gaps in disks in Taurus using the framework of [Zhang et al. \(2018\)](#). In our calculations of the planet frequencies, in contrast to [Zhang et al. \(2023\)](#), we do not exclude any of the proposed planets from the sample, so our numbers may differ from those reported in the original paper. For this sample, the results are consistent with the microlensing FFP population, but only under the assumption that the maximum grain size is $\alpha_{\text{max}} = 1$ cm. Smaller α_{max} leads to larger planets and strong tension with the μFFP population.

5.2.5. ALMA Conclusions

The populations of planets inferred from ALMA gaps prefer a much shallower power-law index ($p \sim 0.5$) than the μFFP population (Figure 6). There are also significantly more giant planets predicted by ALMA gaps than are compatible with the μFFP population. Unlike for direct imaging or radial velocity planets, because these inferred planets are embedded in a protoplanetary disk, they cannot be explained by assigning them to the stellar mass function.

There are several ways this tension might be resolved. First, we have assumed that the inferred ALMA planet populations are representative of the planet population as a whole. [Lodato et al. 2019](#) argues the most significant bias in the Taurus sample is against massive disks (which are likely to have additional massive planets), which supports that assumption. On the other hand, they argue that only 35% of young stars have disks with gaps. This factor of ~ 3 would reduce, but not entirely resolve, the tension with the microlensing results for certain physical assumptions. However, it also requires that planets with $a > 10$ au and $m_p > M_{\text{Sat}}$ are *only* found around stars with disks with gaps.

Another explanation could be that as the systems evolve, the planets migrate away from where they are inferred to form in the protoplanetary disk. However, the migration cannot be outward because those planets would still be detected as part of the μFFP population, even if they are ejected from their host systems. Inward migration would likely require that a significant fraction are absorbed by the star because the number of giant planets at $a < 10$ au has been measured by multiple studies to be $\ll 1$ per star ([Fernandes et al. 2019](#); [Suzuki et al. 2016](#)).

Finally, this tension could suggest problems with the assumed physics of gap formation by planets in these studies. Perhaps there is not a 1-to-1 correspondence between planets and gaps. For example, a single planet may explain multiple gaps in the disk around AS 209 (Fedele et al. 2018). Alternatively, theories about the physical mechanisms controlling gap formation could be incomplete. Regardless, the tension indicates that the μ FFP population has a significant ability to constrain these theories and assumptions.

6. CONCLUSIONS

Data from microlensing (Suzuki et al. 2016; Poleski et al. 2021), radial velocities (Cumming et al. 2008; Mayor et al. 2011; Bonfils et al. 2013), and transits (Lissauer et al. 2023) demonstrate that planets with masses comparable to Saturn and Jupiter are significantly less common than planets with masses comparable to Earth and Neptune. The declining frequency of planets with increasing mass mirrors a similar phenomenon among stars (e.g., Salpeter 1955; Miller & Scalo 1979; Chabrier 2005; Kroupa et al. 2013; Kirkpatrick et al. 2024). From the most massive O-type stars to the lowest mass brown dwarfs, the frequency is a declining function of mass. For stars more massive than $\sim 0.1\text{--}0.2 M_{\odot}$, all derivations of the initial mass function (IMF) agree reasonably well. However, among the lowest mass hydrogen-burning stars and lower mass brown dwarfs, different formulations of the IMF diverge. There is an open question of whether or not the stellar IMF continues into the brown dwarf and planetary mass regime, e.g., as suggested by the discovery of isolated planetary-mass cores in young star-forming regions (e.g., Pearson et al. 2021; Damian et al. 2023).

The mass function (MF) of isolated objects identified with microlensing can be decomposed into two separate components: a free-floating planet (FFP) component and a stellar component (Gould et al. 2022; Sumi et al. 2023). We show that the stellar MF from Sumi et al. (2023) has significantly more objects with $M < 0.1 M_{\odot}$ than the Chabrier (2005) MF, but is similar to the local IMF derived by Kirkpatrick et al. (2024) (see Figure 2). The Sumi et al. (2023) MFs imply that objects with $M \gtrsim 1 M_{\text{Jup}}$ are dominated by objects from the low-mass tail of the stellar mass function, with relatively few objects coming from the high-mass end of planet formation. The conclusions are similar using the Chabrier (2005) stellar MF and the Gould et al. (2022) microlensing FFP (μ FFP) MF, but the transition point shifts to $M \gtrsim 6 M_{\text{Jup}}$.

We compared the microlensing MFs with the populations of companions with masses $m_p > 1 M_{\text{Jup}}$ and semi-major axes $a > 10$ au observed by direct imaging (Nielsen et al. 2019; Vigan et al. 2021, Section 4.1) and radial velocity (Fernandes et al. 2019, Section 4.2). The frequency of these companions is equal to the frequency in the μ FFP population. This result implies that all μ FFPs with these masses are bound planets for which there is no measurable microlensing signal from the host star as hypothesized by Gould et al. (2022). These planets can only exist around more massive stars; there cannot be additional undetected companions around stars outside the ranges probed by those studies. Finally, the microlensing objects from the stellar MF in this mass range should not have host stars, unless the hosts would be undetectable with existing radial velocity or direct imaging surveys.

We predict that if high-resolution imaging is taken for μ FFP candidates with $M > 1 M_{\text{Jup}}$, there must be at least as many host stars with masses $\gtrsim 1 M_{\odot}$ as the number of such candidates predicted to belong to the planetary, rather than stellar, component of the microlensing MF. Alternatively, some fraction of the direct imaging and radial velocity companions are actually brown dwarfs, which formed through the star formation process.

We also conclude that the number of planets with minimum masses $> 1 M_{\text{Sat}}$ inferred from debris disks assuming a single planet maintains the inner edge of the disk (Pearce et al. 2022, Section 5.1) is roughly equal to the number of such planets in the μ FFP MF. This result agrees with our analysis comparing the μ FFP population with radial velocity and direct imaging populations but extending to lower masses: either all μ FFPs must be bound or stars without debris disks tend not to host planets with masses $> 1 M_{\text{Sat}}$ and orbits with $a > 10$ au.

The inferred debris disk planet population extends below $1 M_{\text{Sat}}$. The power-law index for these planets has a much shallower slope than the μ FFP MF. The μ FFP population can easily accommodate this population of smaller planets and additional contributions from smaller planets, including those around stars without debris disks or ejected planets. At the same time, the planet masses from Pearce et al. (2022) are lower limits, but if they were much larger, they would violate the constraints from the higher mass μ FFP population. Hence, the μ FFP population constrains the masses of the population of planets sculpting debris disks or suggests that they are sculpted by multiple, smaller planets, an alternative hypothesis investigated by Pearce et al. (2022).

In addition, the μ FFP population is not consistent with the hypothesis that every ALMA gap contains a planet (Zhang et al. 2018; Lodato et al. 2019; Wang et al. 2021; Zhang et al. 2023, Section 5.2). Even if we account for the possibility that only stars with massive disks host such planets, the required numbers of $m_p > 1 M_{\text{Sat}}$ are in tension

with the μ FFP population. Because the μ FFP population constrains all objects with $a > 10$ au, migration can only resolve this tension if the planets migrate inward. In that case, a large fraction would have to be absorbed by their stars due to the constraints on the frequency of giant planets with $a < 10$ au. More plausibly, there is not a 1-to-1 correspondence between ALMA gaps and planets. Instead, these results favor a scenario in which a single planet induces multiple gaps.

These comparisons demonstrate the power of microlensing measurements of the mass function to constrain the wide-orbit planet population and the physics governing structures in circumstellar disks. Stronger comparisons would be possible with larger samples of direct imaging and radial velocity planets, which would allow more precise frequency measurements as a function of companion mass, and a better understanding of the range of host star masses that are probed by direct imaging and ALMA disk studies.

ACKNOWLEDGEMENTS

J.C.Y. acknowledges support from U.S. NSF Grant No. AST-2108414.

This research has made use of the NASA Exoplanet Archive, which is operated by the California Institute of Technology, under contract with the National Aeronautics and Space Administration under the Exoplanet Exploration Program.

REFERENCES

- ALMA Partnership, Brogan, C. L., Pérez, L. M., et al. 2015, *ApJL*, 808, L3, doi: [10.1088/2041-8205/808/1/L3](https://doi.org/10.1088/2041-8205/808/1/L3)
- Andrews, S. M., Wilner, D. J., Zhu, Z., et al. 2016, *ApJL*, 820, L40, doi: [10.3847/2041-8205/820/2/L40](https://doi.org/10.3847/2041-8205/820/2/L40)
- Andrews, S. M., Huang, J., Pérez, L. M., et al. 2018, *ApJL*, 869, L41, doi: [10.3847/2041-8213/aaf741](https://doi.org/10.3847/2041-8213/aaf741)
- Avenhaus, H., Quanz, S. P., Garufi, A., et al. 2018, *ApJ*, 863, 44, doi: [10.3847/1538-4357/aab846](https://doi.org/10.3847/1538-4357/aab846)
- Bae, J., Isella, A., Zhu, Z., et al. 2023, in *Astronomical Society of the Pacific Conference Series*, Vol. 534, *Protostars and Planets VII*, ed. S. Inutsuka, Y. Aikawa, T. Muto, K. Tomida, & M. Tamura, 423, doi: [10.48550/arXiv.2210.13314](https://doi.org/10.48550/arXiv.2210.13314)
- Bae, J., Pinilla, P., & Birnstiel, T. 2018, *ApJL*, 864, L26, doi: [10.3847/2041-8213/aadd51](https://doi.org/10.3847/2041-8213/aadd51)
- Bond, I. A., Udalski, A., Jaroszyński, M., et al. 2004, *ApJL*, 606, L155, doi: [10.1086/420928](https://doi.org/10.1086/420928)
- Bonfils, X., Delfosse, X., Udry, S., et al. 2013, *A&A*, 549, A109, doi: [10.1051/0004-6361/201014704](https://doi.org/10.1051/0004-6361/201014704)
- Bowler, B. P., Liu, M. C., Shkolnik, E. L., & Tamura, M. 2015, *ApJS*, 216, 7, doi: [10.1088/0067-0049/216/1/7](https://doi.org/10.1088/0067-0049/216/1/7)
- Bowler, B. P., Zhou, Y., Biddle, L. I., et al. 2025, *arXiv e-prints*, arXiv:2502.14736, doi: [10.48550/arXiv.2502.14736](https://doi.org/10.48550/arXiv.2502.14736)
- Burrows, A., Marley, M., Hubbard, W. B., et al. 1997, *ApJ*, 491, 856, doi: [10.1086/305002](https://doi.org/10.1086/305002)
- Chabrier, G. 2005, in *Astrophysics and Space Science Library*, Vol. 327, *The Initial Mass Function 50 Years Later*, ed. E. Corbelli, F. Palla, & H. Zinnecker, 41, doi: [10.1007/978-1-4020-3407-7_5](https://doi.org/10.1007/978-1-4020-3407-7_5)
- Cieza, L. A., Ruíz-Rodríguez, D., Hales, A., et al. 2019, *MNRAS*, 482, 698, doi: [10.1093/mnras/sty2653](https://doi.org/10.1093/mnras/sty2653)
- Cimernan, N. P., & Rafikov, R. R. 2021, *MNRAS*, 508, 2329, doi: [10.1093/mnras/stab2652](https://doi.org/10.1093/mnras/stab2652)
- Clanton, C., & Gaudi, B. S. 2016, *ApJ*, 819, 125, doi: [10.3847/0004-637X/819/2/125](https://doi.org/10.3847/0004-637X/819/2/125)
- . 2017, *ApJ*, 834, 46, doi: [10.3847/1538-4357/834/1/46](https://doi.org/10.3847/1538-4357/834/1/46)
- Close, L. M., Males, J. R., Li, J., et al. 2025, *AJ*, 169, 35, doi: [10.3847/1538-3881/ad8648](https://doi.org/10.3847/1538-3881/ad8648)
- Cumming, A., Butler, R. P., Marcy, G. W., et al. 2008, *PASP*, 120, 531, doi: [10.1086/588487](https://doi.org/10.1086/588487)
- Currie, T., Biller, B., Lagrange, A., et al. 2023, in *Astronomical Society of the Pacific Conference Series*, Vol. 534, *Protostars and Planets VII*, ed. S. Inutsuka, Y. Aikawa, T. Muto, K. Tomida, & M. Tamura, 799, doi: [10.48550/arXiv.2205.05696](https://doi.org/10.48550/arXiv.2205.05696)
- Damian, B., Jose, J., Biller, B., et al. 2023, *ApJ*, 951, 139, doi: [10.3847/1538-4357/acd115](https://doi.org/10.3847/1538-4357/acd115)
- Dong, R., Rafikov, R. R., & Stone, J. M. 2011, *ApJ*, 741, 57, doi: [10.1088/0004-637X/741/1/57](https://doi.org/10.1088/0004-637X/741/1/57)
- Drazkowska, J., Bitsch, B., Lambrechts, M., et al. 2023, in *Astronomical Society of the Pacific Conference Series*, Vol. 534, *Protostars and Planets VII*, ed. S. Inutsuka, Y. Aikawa, T. Muto, K. Tomida, & M. Tamura, 717, doi: [10.48550/arXiv.2203.09759](https://doi.org/10.48550/arXiv.2203.09759)
- Esposito, T. M., Kalas, P., Fitzgerald, M. P., et al. 2020, *AJ*, 160, 24, doi: [10.3847/1538-3881/ab9199](https://doi.org/10.3847/1538-3881/ab9199)
- Fedele, D., Tazzari, M., Booth, R., et al. 2018, *A&A*, 610, A24, doi: [10.1051/0004-6361/201731978](https://doi.org/10.1051/0004-6361/201731978)
- Fernandes, R. B., Mulders, G. D., Pascucci, I., Mordasini, C., & Emsenhuber, A. 2019, *ApJ*, 874, 81, doi: [10.3847/1538-4357/ab0300](https://doi.org/10.3847/1538-4357/ab0300)

- Friebe, M. F., Pearce, T. D., & Löhne, T. 2022, *MNRAS*, 512, 4441, doi: [10.1093/mnras/stac664](https://doi.org/10.1093/mnras/stac664)
- Fulton, B. J., Rosenthal, L. J., Hirsch, L. A., et al. 2021, *ApJS*, 255, 14, doi: [10.3847/1538-4365/abfcc1](https://doi.org/10.3847/1538-4365/abfcc1)
- Gaudi, B. S. 2012, *ARA&A*, 50, 411, doi: [10.1146/annurev-astro-081811-125518](https://doi.org/10.1146/annurev-astro-081811-125518)
- Gould, A. 2016, *Journal of Korean Astronomical Society*, 49, 123, doi: [10.5303/JKAS.2016.49.4.123](https://doi.org/10.5303/JKAS.2016.49.4.123)
- Gould, A., Dong, S., Gaudi, B. S., et al. 2010, *ApJ*, 720, 1073, doi: [10.1088/0004-637X/720/2/1073](https://doi.org/10.1088/0004-637X/720/2/1073)
- Gould, A., Jung, Y. K., Hwang, K.-H., et al. 2022, *Journal of Korean Astronomical Society*, 55, 173, doi: [10.5303/JKAS.2022.55.5.173](https://doi.org/10.5303/JKAS.2022.55.5.173)
- Huang, J., Ansdell, M., Birnstiel, T., et al. 2024, *ApJ*, 976, 132, doi: [10.3847/1538-4357/ad84df10.1134/S10663773708080094](https://doi.org/10.3847/1538-4357/ad84df10.1134/S10663773708080094)
- Huang, J., Andrews, S. M., Dullemond, C. P., et al. 2018, *ApJL*, 869, L42, doi: [10.3847/2041-8213/aaf740](https://doi.org/10.3847/2041-8213/aaf740)
- Hughes, A. M., Duchêne, G., & Matthews, B. C. 2018, *ARA&A*, 56, 541, doi: [10.1146/annurev-astro-081817-052035](https://doi.org/10.1146/annurev-astro-081817-052035)
- Jung, Y. K., Hwang, K.-H., Yang, H., et al. 2024, *AJ*, 168, 152, doi: [10.3847/1538-3881/ad6b12](https://doi.org/10.3847/1538-3881/ad6b12)
- Kanagawa, K. D., Muto, T., Tanaka, H., et al. 2016, *PASJ*, 68, 43, doi: [10.1093/pasj/psw037](https://doi.org/10.1093/pasj/psw037)
- Kim, H.-W., Hwang, K.-H., Gould, A., et al. 2021, *AJ*, 162, 15, doi: [10.3847/1538-3881/abfc4a](https://doi.org/10.3847/1538-3881/abfc4a)
- Kim, S.-L., Lee, C.-U., Park, B.-G., et al. 2016, *Journal of Korean Astronomical Society*, 49, 37, doi: [10.5303/JKAS.2016.49.1.037](https://doi.org/10.5303/JKAS.2016.49.1.037)
- Kirkpatrick, J. D., Marocco, F., Gelino, C. R., et al. 2024, *ApJS*, 271, 55, doi: [10.3847/1538-4365/ad24e2](https://doi.org/10.3847/1538-4365/ad24e2)
- Koshimoto, N., Sumi, T., Bennett, D. P., et al. 2023, *AJ*, 166, 107, doi: [10.3847/1538-3881/ace689](https://doi.org/10.3847/1538-3881/ace689)
- Kroupa, P., Weidner, C., Pflamm-Altenburg, J., et al. 2013, in *Planets, Stars and Stellar Systems. Volume 5: Galactic Structure and Stellar Populations*, ed. T. D. Oswalt & G. Gilmore, Vol. 5 (Springer, Dordrecht), 115, doi: [10.1007/978-94-007-5612-0_4](https://doi.org/10.1007/978-94-007-5612-0_4)
- Lafrenière, D., Doyon, R., Marois, C., et al. 2007, *ApJ*, 670, 1367, doi: [10.1086/522826](https://doi.org/10.1086/522826)
- Lagrange, A. M., Philipot, F., Rubini, P., et al. 2023, *A&A*, 677, A71, doi: [10.1051/0004-6361/202346165](https://doi.org/10.1051/0004-6361/202346165)
- Lagrange, A.-M., Gratadour, D., Chauvin, G., et al. 2009, *A&A*, 493, L21, doi: [10.1051/0004-6361:200811325](https://doi.org/10.1051/0004-6361:200811325)
- Lagrange, A. M., Meunier, N., Rubini, P., et al. 2019, *Nature Astronomy*, 3, 1135, doi: [10.1038/s41550-019-0857-1](https://doi.org/10.1038/s41550-019-0857-1)
- Lestrade, J. F., Wyatt, M. C., Bertoldi, F., Menten, K. M., & Labaigt, G. 2009, *A&A*, 506, 1455, doi: [10.1051/0004-6361/200912306](https://doi.org/10.1051/0004-6361/200912306)
- Lissauer, J. J., Batalha, N. M., & Borucki, W. J. 2023, in *Astronomical Society of the Pacific Conference Series*, Vol. 534, *Protostars and Planets VII*, ed. S. Inutsuka, Y. Aikawa, T. Muto, K. Tomida, & M. Tamura, 839, doi: [10.48550/arXiv.2311.04981](https://doi.org/10.48550/arXiv.2311.04981)
- Lodato, G., Dipierro, G., Ragusa, E., et al. 2019, *MNRAS*, 486, 453, doi: [10.1093/mnras/stz913](https://doi.org/10.1093/mnras/stz913)
- Long, F., Herczeg, G. J., Harsono, D., et al. 2019, *ApJ*, 882, 49, doi: [10.3847/1538-4357/ab2d2d](https://doi.org/10.3847/1538-4357/ab2d2d)
- Marois, C., Macintosh, B., Barman, T., et al. 2008, *Science*, 322, 1348, doi: [10.1126/science.1166585](https://doi.org/10.1126/science.1166585)
- Marois, C., Zuckerman, B., Konopacky, Q. M., Macintosh, B., & Barman, T. 2010, *Nature*, 468, 1080, doi: [10.1038/nature09684](https://doi.org/10.1038/nature09684)
- Mayor, M., Marmier, M., Lovis, C., et al. 2011, *arXiv e-prints*, arXiv:1109.2497, <https://arxiv.org/abs/1109.2497>
- Michel, A., Sadavoy, S. I., Sheehan, P. D., et al. 2023, *AJ*, 166, 184, doi: [10.3847/1538-3881/acf653](https://doi.org/10.3847/1538-3881/acf653)
- Miller, G. E., & Scalo, J. M. 1979, *ApJS*, 41, 513, doi: [10.1086/190629](https://doi.org/10.1086/190629)
- Montet, B. T., Crepp, J. R., Johnson, J. A., Howard, A. W., & Marcy, G. W. 2014, *ApJ*, 781, 28, doi: [10.1088/0004-637X/781/1/28](https://doi.org/10.1088/0004-637X/781/1/28)
- Mróz, P., Ban, M., Marty, P., & Poleski, R. 2024, *AJ*, 167, 40, doi: [10.3847/1538-3881/ad1106](https://doi.org/10.3847/1538-3881/ad1106)
- Mróz, P., Udalski, A., Skowron, J., et al. 2017, *Nature*, 548, 183, doi: [10.1038/nature23276](https://doi.org/10.1038/nature23276)
- Mróz, P., Ryu, Y.-H., Skowron, J., et al. 2018, *AJ*, 155, 121, doi: [10.3847/1538-3881/aaae9](https://doi.org/10.3847/1538-3881/aaae9)
- Mróz, P., Udalski, A., Bennett, D. P., et al. 2019, *A&A*, 622, A201, doi: [10.1051/0004-6361/201834557](https://doi.org/10.1051/0004-6361/201834557)
- Mróz, P., Poleski, R., Gould, A., et al. 2020a, *ApJL*, 903, L11, doi: [10.3847/2041-8213/abfbad](https://doi.org/10.3847/2041-8213/abfbad)
- Mróz, P., Poleski, R., Han, C., et al. 2020b, *AJ*, 159, 262, doi: [10.3847/1538-3881/ab8aeb](https://doi.org/10.3847/1538-3881/ab8aeb)
- Najita, J. R., Kenyon, S. J., & Bromley, B. C. 2022, *ApJ*, 925, 45, doi: [10.3847/1538-4357/ac37b6](https://doi.org/10.3847/1538-4357/ac37b6)
- Nielsen, E. L., De Rosa, R. J., Macintosh, B., et al. 2019, *AJ*, 158, 13, doi: [10.3847/1538-3881/ab16e9](https://doi.org/10.3847/1538-3881/ab16e9)
- Paczynski, B. 1986, *ApJ*, 304, 1, doi: [10.1086/164140](https://doi.org/10.1086/164140)
- Pearce, T. D., Launhardt, R., Ostermann, R., et al. 2022, *A&A*, 659, A135, doi: [10.1051/0004-6361/202142720](https://doi.org/10.1051/0004-6361/202142720)
- Pearson, S., Scholz, A., Teixeira, P. S., Mužić, K., & Almindros-Abad, V. 2021, *MNRAS*, 507, 4074, doi: [10.1093/mnras/stab2394](https://doi.org/10.1093/mnras/stab2394)

- Pecaut, M. J., & Mamajek, E. E. 2013, *ApJS*, 208, 9, doi: [10.1088/0067-0049/208/1/9](https://doi.org/10.1088/0067-0049/208/1/9)
- Pineda, J. E., Arzoumanian, D., Andre, P., et al. 2023, in *Astronomical Society of the Pacific Conference Series*, Vol. 534, *Protostars and Planets VII*, ed. S. Inutsuka, Y. Aikawa, T. Muto, K. Tomida, & M. Tamura, 233, doi: [10.48550/arXiv.2205.03935](https://doi.org/10.48550/arXiv.2205.03935)
- Poleski, R., Skowron, J., Mróz, P., et al. 2021, *AcA*, 71, 1, doi: [10.32023/0001-5237/71.1.1](https://doi.org/10.32023/0001-5237/71.1.1)
- Rosenthal, L. J., Fulton, B. J., Hirsch, L. A., et al. 2021, *ApJS*, 255, 8, doi: [10.3847/1538-4365/abe23c](https://doi.org/10.3847/1538-4365/abe23c)
- Ryu, Y.-H., Mróz, P., Gould, A., et al. 2021, *AJ*, 161, 126, doi: [10.3847/1538-3881/abd55f](https://doi.org/10.3847/1538-3881/abd55f)
- Salpeter, E. E. 1955, *ApJ*, 121, 161, doi: [10.1086/145971](https://doi.org/10.1086/145971)
- Schlaufman, K. C. 2018, *ApJ*, 853, 37, doi: [10.3847/1538-4357/aa961c](https://doi.org/10.3847/1538-4357/aa961c)
- Sheehan, P. D., Tobin, J. J., Federman, S., Megeath, S. T., & Looney, L. W. 2020, *ApJ*, 902, 141, doi: [10.3847/1538-4357/abbad5](https://doi.org/10.3847/1538-4357/abbad5)
- Shu, F. H., Adams, F. C., & Lizano, S. 1987, *ARA&A*, 25, 23, doi: [10.1146/annurev.aa.25.090187.000323](https://doi.org/10.1146/annurev.aa.25.090187.000323)
- Smallwood, J. L., Yang, C.-C., Zhu, Z., et al. 2023, *MNRAS*, 521, 3500, doi: [10.1093/mnras/stad742](https://doi.org/10.1093/mnras/stad742)
- Stuber, T. A., Löhne, T., & Wolf, S. 2023, *A&A*, 669, A3, doi: [10.1051/0004-6361/202243240](https://doi.org/10.1051/0004-6361/202243240)
- Sumi, T., Bennett, D. P., Bond, I. A., et al. 2010, *ApJ*, 710, 1641, doi: [10.1088/0004-637X/710/2/1641](https://doi.org/10.1088/0004-637X/710/2/1641)
- Sumi, T., Kamiya, K., Bennett, D. P., et al. 2011, *Nature*, 473, 349, doi: [10.1038/nature10092](https://doi.org/10.1038/nature10092)
- Sumi, T., Koshimoto, N., Bennett, D. P., et al. 2023, *AJ*, 166, 108, doi: [10.3847/1538-3881/ace688](https://doi.org/10.3847/1538-3881/ace688)
- Suzuki, D., Bennett, D. P., Sumi, T., et al. 2016, *ApJ*, 833, 145, doi: [10.3847/1538-4357/833/2/145](https://doi.org/10.3847/1538-4357/833/2/145)
- Teague, R., Bae, J., Aikawa, Y., et al. 2021, *ApJS*, 257, 18, doi: [10.3847/1538-4365/ac1438](https://doi.org/10.3847/1538-4365/ac1438)
- van der Marel, N., & Mulders, G. D. 2021, *AJ*, 162, 28, doi: [10.3847/1538-3881/ac0255](https://doi.org/10.3847/1538-3881/ac0255)
- van der Marel, N., Birnstiel, T., Garufi, A., et al. 2021, *AJ*, 161, 33, doi: [10.3847/1538-3881/abc3ba](https://doi.org/10.3847/1538-3881/abc3ba)
- Vigan, A., Fontanive, C., Meyer, M., et al. 2021, *A&A*, 651, A72, doi: [10.1051/0004-6361/202038107](https://doi.org/10.1051/0004-6361/202038107)
- Vorobyov, E. I., Skliarevskii, A. M., Elbakyan, V. G., et al. 2020, *A&A*, 635, A196, doi: [10.1051/0004-6361/201936990](https://doi.org/10.1051/0004-6361/201936990)
- Wang, S., Kanagawa, K. D., & Suto, Y. 2021, *ApJ*, 923, 165, doi: [10.3847/1538-4357/ac2d95](https://doi.org/10.3847/1538-4357/ac2d95)
- Wittenmyer, R. A., Wang, S., Horner, J., et al. 2020, *MNRAS*, 492, 377, doi: [10.1093/mnras/stz3436](https://doi.org/10.1093/mnras/stz3436)
- Yoo, J., DePoy, D. L., Gal-Yam, A., et al. 2004, *ApJ*, 603, 139, doi: [10.1086/381241](https://doi.org/10.1086/381241)
- Zhang, S., Kalscheur, M., Long, F., et al. 2023, *ApJ*, 952, 108, doi: [10.3847/1538-4357/acd334](https://doi.org/10.3847/1538-4357/acd334)
- Zhang, S., Zhu, Z., Huang, J., et al. 2018, *The Astrophysical Journal*, 869, L47, doi: [10.3847/2041-8213/aaf744](https://doi.org/10.3847/2041-8213/aaf744)
- Zhou, Y., Bowler, B. P., Sanghi, A., et al. 2025, *ApJL*, 980, L39, doi: [10.3847/2041-8213/adb134](https://doi.org/10.3847/2041-8213/adb134)